Bioceramics Development and Applications
ISSN: 2090-5025

Hogga et al., Bioceram Dev Appl 2016, 6:1
DOI: 10.4172/2090-5025.100092

Research Article Open Access

Variable-Temperature Measurements of the Dielectric Relaxation Spectroscopy in 0.1 SiO_2-0.2 Cao-0.2 Na_2O-0.5 P_2O_5 Bioactive Glass Materials

Hogga Z[1], Merzouk N[2] and Hafid MM[1]*

[1]*Laboratory of Engineering and Environmental studies, Department of Physics, Faculty of sciences, University of Ibn Tofail, 14000 Kenitra, Morocco*
[2]*Faculty of Dental Medicine, Rabat, Morocco*

Abstract

Bioactive glasses with chemical composition 0.1 SiO_2-0.2 CaO-0.2 Na_2O-0.5 P_2O_5 have been prepared. The dielectric properties of the samples were measured in the frequency range from 100 Hz to 1 MHz and temperatures range from 100 to 370 K (Tg ≈ 400 K). The obtained data were analysed by the means of dielectric permittivity representation and modelled using the Havriliak–Negami equation. Various relaxation parameters were calculated with accuracy. Furthermore, investigation of the temperature dependence of their relaxation time using the Vogel–Tammam–Fulcher (VTF) model shows the weak interaction between alkali ions constituents and molecular network-formers for temperatures up to the glass transition.

Keywords: Amorphous materials; Composite; Chemical synthesis; Differential Scanning Calorimetry (DSC); Dielectric properties; Impedance spectroscopy electrical properties

Introduction

In the recent years, there is increasing demands of using and understanding bioglass materials for scientific research and industrials [1]. Silicate and phosphate glasses have been carried out with the aim to control physical, chemical and biological properties, such as second-order nonlinear optical susceptibility and bioactivity, they have also found application as biomaterials to replace or repair hard or soft tissues [2-5]. Phosphosilicate based glasses produce a bonelike apatite layer on its surface when interacting with host medium [6-8]. Recently, researchers have been focusing on the bioactive phosphate glasses because they are unique class of materials that are biodegradable and biocompatible, and their degradation can be tailored for varying from days to several months as bone implant by changing the glass modifiers and preparation techniques [9,10]. By suitably altering the composition, the glass network modifier oxides like CaO and Na_2O are added to phosphosilicate composite network in order to improve its electrical transport properties and to control the degree of solubility of bioactive glass in a physiological environment [11]. Further, the solubility of the bioactive glass has been directly linked to the ionic release from the material to the host medium. Hence the understanding of the alkali ion transport mechanism of the bioglass is very important. The dynamics of charges can be studied by analytical technique of alternating current impedance spectroscopy which has been considered as the best tool for understanding the dynamics of alkali ions in the bioactive glass [12]. The real and imaginary parts, of the dynamics modulus formalism and complex impedance representation of phosphate-silicate bioactive glass has been studied, respectively, by Mai et al. and Mariappan et al. they suggest that the observed relaxations in the bioactive glass may be more appropriately considered as an intrinsic property of the non-periodic arrangement of atoms or ions in a solid than as being due to the diffusion of specific types of ions in it [13,14].

Dielectric relaxation and related phenomena are present in this bioactive glass and their investigation is essential not only from the practical point of view due to the potential application, but also for the insight information that can provide referring to molecular/ions mobility, polarization and conductivity mechanisms [15-17]. These amorphous bioactive glasses are formed by the mixture of the merit compositions of silicate-phosphate as a network formers and sodium-calcium network modifiers powders which are considered as disordered system and many equations have been proposed for describing their behavior in terms of the permittivity of their constituents.

The aim of this study was to investigate the dielectric relaxation behaviour and electrical mobility of the phosphosilicate bioglass composite containing 0.1 SiO_2-0.2 CaO 0.2 Na_2O-0.5 P_2O_5 and to their modelling. The relaxation phenomenon exhibited by the sample in the range from 100 Hz to 1 MHz was studied as a function of the temperature below the glass transition point T_g. In order hand, it is known that glass-forming materials are characterized by a number of unusual properties, which seem to be inherent to the glassy state of matter and which are quite universally found in such different types of materials [18-20]. May be the most prominent examples are the non-exponential time dependence of their relaxation behaviour and the non-Arrhenius temperature dependence of their structural relaxation dynamics [21]. Furthermore, there are numerous competing theoretical models of the glass transition that can describe the observed behavior with various levels of precision and the glass-physics community still is far from reaching any consensus in the settlement of this question [22-24].

In our case and in order to parameterize the obtained results on the temperature-dependent relaxation, we revert to the most prominent

***Corresponding authors:** Hafid MM, Laboratory of Engineering and Environment studies, Department of Physics, Faculty of sciences, University of Ibn Tofail, 14000 Kenitra, Morocco, Tel: +212537329292, Fax: +212537329290; E-mail: mymustaphahafid@gmail.com

Received April 28, 2016; **Accepted** May 17, 2016; **Published** May 23, 2016

Citation: Hogga Z, Merzouk N, Hafid MM (2016) Variable-Temperature Measurements of the Dielectric Relaxation Spectroscopy in 0.1 SiO_2-0.2 Cao-0.2 Na_2O-0.5 P_2O_5 Bioactive Glass Materials. Bioceram Dev Appl 6: 092. doi:10.4172/2090-5025.100092

Vogel-Fulcher-Tammann (VFT) law phenomenological approach [25].

Experimental Techniques

Sample preparation

Sample of phosphosilicate bioactive glass with chemical composition 0.1 SiO_2-0.2 CaO-0.2 Na_2O-0.5 P_2O_5 was prepared from Na_2CO_3 (99.98%), $CaCO_3$ (100%), SiO_2 (99.9%) and $(NH_4)_2HPO_4$ (99.8%) powders. Initially, they reagents $(NH_4)_2HPO_4$, Na_2CO_3 and $CaCO_3$ were kept in an oven and tried at 400 K for 12 hours in order to remove any traces of water and absorbed gases CO_2 and NO_2. Then stoichiometric amounts of the starting materials were weighed by using digital electronic balance and were grounds in a gate mortar for a few minutes. The mixtures were placed in alumina crucible and melted in an electric furnace at 1100 K for one hour. After complete homogenization, the melt was poured into preheated stainless steel mold with a cylindrical shape.

Measurements

Differential scanning calorimetry (DSC) measurement was performed on a DSC 121 RM under an Ar flux and a heating rate of 10°C/min. For the dielectric measurements, the sample were prepared as a disc with a thickness of about 1 mm. Aluminium electrodes of 10 mm diameter were deposited on the opposite sides of the samples. The electrical leads were fixed by silver paint. The dielectric measurements were carried out, in the frequency range from 100 Hz to 0.2 MHz, using a SR850 DSP Lock-In Amplifier, in the typical lock-in configuration. We measured the "in-phase" (V_f) and the "out-of phase" (Vq) components of the sample signal, and then we calculated the real and imaginary parts of the complex impedance $Z^*(\omega)$, using the expressions:

$$Z'(\omega) = \frac{R_i(V_f V_0 - V_f^2 - V_q^2) - \omega C_i^2 R_i^2 V_q V_0}{(1+\omega^2 C_i^2 R_i^2)(V_f^2 + V_q^2)} \quad (a)$$

$$Z''(\omega) = \frac{V_q V_0 R_i + \omega C_i^2 R_i^2 (V_f V_0 - V_f^2 - V_q^2)}{(1+\omega^2 C_i^2 R_i^2)(V_f^2 + V_q^2)} \quad (b)$$

Where ω is the angular frequency. This equation was obtained when the sample impedance is in series with a known resistance (1 kΩ), which is in parallel with the lock-in input impedance. R_i represents the equivalent resistance of the lock-in input resistance (100 MΩ) and the known resistance, C_i the lock-in input capacitance (15 pF), V_0 the input signal ($|V_0|$=1 V), and V_f and V_q the "in-phase" and the "out-of-phase" components of the measured signal. The sample was modeled by a lumped circuit consisting of a resistance and a capacitor in parallel. The complex admittance $Y^*(\omega) = 1/Z^*(\omega) = G(\omega) + jB(\omega)$ can be converted into complex permittivity formalism $\varepsilon^*(\omega) = \varepsilon'(\omega) - j\varepsilon''(\omega)$ by the relations:

$$\varepsilon'(\omega) = \frac{B(\omega).e}{\varepsilon_0 A\omega} \quad (c)$$

$$\varepsilon''(\omega) = \frac{G(\omega).e}{\varepsilon_0 A\omega} \quad (d)$$

where A is the cross-sectional area of the sample, e is its thickness and ε_0 is the permittivity of a vacuum (ε_0 = 8.85 x 10^{-12} F m^{-1}). The terms $G(\omega)$ and $B(\omega)$ are respectively the conductance and the susceptance of the samples. Estimating relative errors on both real and imaginary part of the complex permittivity are: $\Delta\varepsilon'/\varepsilon' = \Delta\varepsilon''/\varepsilon'' \leq 5\%$.

Results and Discussion

X-ray and DSC analysis

The X-ray diffraction pattern shows no crystalline phases in the bioglass sample. Figure 1 presents the diffraction spectrum of the sample; this latter is amorphous as indicated by the absence of Bragg peaks and presence of amorphous halos.

Figure 2 shows the heating DSC thermogram of the bioglass sample. At about 420 K a change in the base line is observed. This phenomenon is attributed to the glass transition temperature Tg. This measurement indicates that the glass transition temperature T_g, which is associated to the transition from a glass like form to a rubbery. It should be reminded that the determination of T_g, in our case, was carried out according to the method of the tangents. As, in general, a glass transition involves a small flow of heat, the detected variations of capacity calorific or enthalpy are also small, and for this, the determination is not very accurate.

Analysis of dielectric spectrum and modeling

The study of frequency dependent permittivity spectra is a well-established method for characterizing the hopping dynamics of ions. Frequency dependence on real (ε′) and imaginary (ε″) parts of the effective dielectric permittivity ε* spectra at various temperatures of the phosphosilicate bioglass composite containing 0.1SiO_2-0.2CaO-0.2Na_2O-0.5P_2O_5 are shown in Figure 3. The appearance of broad dielectric relaxations for temperature below T_g on the isothermal runs of the loss factor is presented in these measurements, as shown in Figure 3a, it is observed that the low-frequency value of ε′ is high reaches to ε_s which decreases with increasing frequency and reaches a minimum asymptotic value ε_∞ at high frequency. The ε″ spectrum in Figure 3b exhibits a maximum ε_m^* centred in dispersion region of ε′ and the peak position is shifted to the high frequency side with increasing temperature. From aforementioned analysis, one can conclude that the

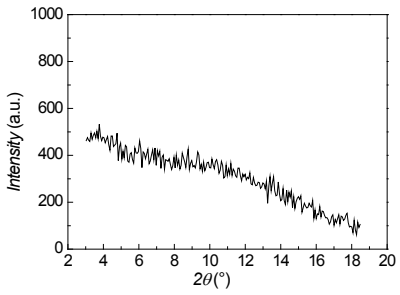

Figure 1: Typical X-ray diffraction pattern of the bioglass sample.

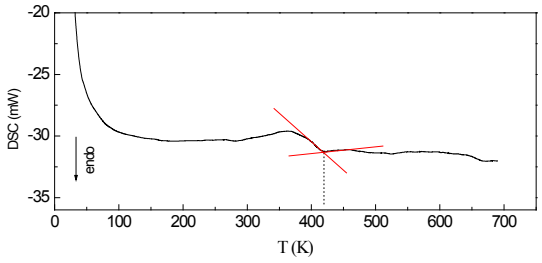

Figure 2: Temperature dependence of the DSC signal for bioglass sample.

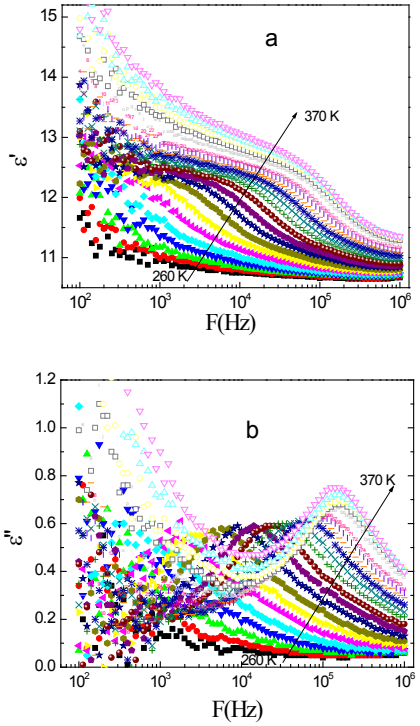

Figure 3: Real ε′(a) and imaginary ε″(b) parts of the complex permittivity vs. frequency for the sample in the temperature range (260K - 370K).

frequency region below the peak maximum of ε″ determines the range in which charge carriers are mobile over long distances and in the region above the peak maximum the carriers are confined to potential wells being mobile over short distances [26,27].

For modeling these behaviors, we used the Nyquist diagram representation, as depicted in Figure 4a. The unsymmetrical profile of ε″ indicates that the single relaxation time as described by the Debye equation is inappropriate for describing the electrical relaxation and should be replaced by Havriliak-Negami (HN) phenomenology [28]:

$$\frac{\varepsilon^*(\omega)-\varepsilon_\infty}{\varepsilon_s-\varepsilon_\infty}=\frac{1}{\left(1+(i\omega\tau)^\alpha\right)^\beta} \quad (1)$$

Where the positive constants ε_s and ε_∞ denote the static ($\omega = 0$) and the high frequency values of the permittivity, respectively. ω denotes the angular frequency ($\omega = 2\pi F$), τ is the relaxation time of the composite, α is the shape parameter representing symmetrical distribution of relaxation time and β is the shape parameter of an asymmetric relaxation curve. The maximum frequency of the relaxation peak in $\varepsilon^*(\omega)$ is approximately situated at $1/2\pi\tau$. The width parameter α specifies the slope of the low frequency side of the relaxation and $-\alpha\beta$ gives the slope of the high frequency side of the relaxation in $\varepsilon''(\omega)$ [21]. The Havriliak-Negami (HN) equation includes the Debye model for ($\alpha = \beta = 1$), Cole-Cole model (CC) for ($\beta = 1$) and Cole-Davidson (CD) model for ($\alpha = 1$).

Our goal now is to assess with accuracy the behavior of ε*(ω) according to the HN model. One of the most popular ansatz for the relaxation in dielectric materials is given by the HN phenomenology (Equation 1). Figure 4b shows an example of the (ε″, ε′) vs. frequency and ε″ vs. ε′ data along with a simulation (solid line) based on the HN modeling for the dielectric permittivity. The basic functional form of ε^* is well known and can be expressed as:

$$\frac{\varepsilon'(\omega)-\varepsilon_\infty}{\varepsilon_s-\varepsilon_\infty}=\frac{\cos(\beta\phi)}{\left(1+2(\omega\tau)^\alpha\cos(\frac{\alpha\pi}{2})+(\omega\tau)^{2\alpha}\right)^{\beta/2}} \quad (2)$$

$$\frac{\varepsilon''(\omega)}{\varepsilon_s-\varepsilon_\infty}=\frac{\sin(\beta\phi)}{\left(1+2(\omega\tau)^\alpha\cos(\frac{\alpha\pi}{2})+(\omega\tau)^{2\alpha}\right)^{\beta/2}} \quad (3)$$

Where

$$\phi=\tan^{-1}\left(\frac{(\omega\tau)^\alpha\sin(\frac{\alpha\pi}{2})}{1+(\omega\tau)^\alpha\cos(\frac{\alpha\pi}{2})}\right) \quad (4)$$

We performed a fit to the data using the Equations (2-4) for ε′ and ε″ from which we extract the parameters α and β which gauge the broadening of the loss spectrum. Figure 5 shows the evolutions of the relaxation parameters with temperature, it appears that the behavior of the parameters α and β reveal that dielectric data are best fitted according to the CD model at low temperatures (T < 300 K) and according to the CC model for high temperatures (T > 350 K). The decrease of α and increase of β with increasing of temperature indicating that the system departs from the Debye model this behavior is due to the changing dynamics of dipole clusters in low temperature and to alkali ion dynamics in network bioactive glasses. Indeed, the temperature-dependence of relaxation times reveals a steadily decreasing behavior due to an increase molecular dipoles mobility as temperature increases, for a higher temperature (T > 350 K), the relaxation time does not depend of temperature which indicate that the mechanism does not result simply from thermally activated dipolar interactions but may be also related to a cooperative effect of network modifiers (alkali ions)

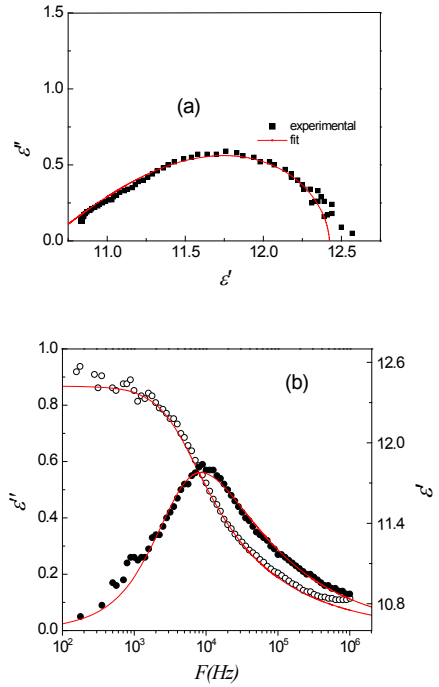

Figure 4: (a) Nyquist plot of the same sample. (b) Plot of ε″ and ε′ as a function of frequency at room temperature. The solid curve is produced by best fitting experimental points using the Equations.(2-4), the fit parameters are τ = 3.77 10^{-5} s, α = 0.95 and β = 0.44.

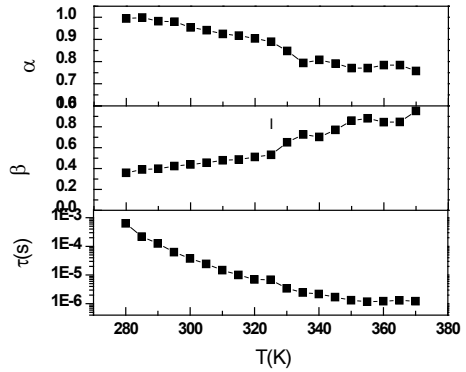

Figure 5: Temperature dependence of relaxations parameters obtained from the fitting of data using H-N model.

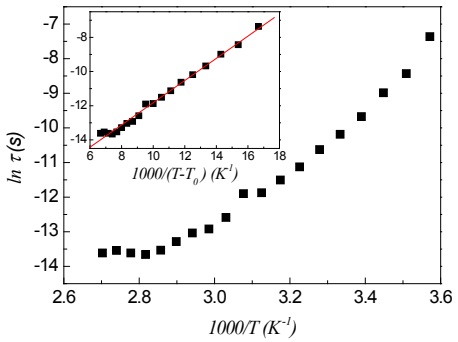

Figure 6: *ln*(τ) vs. 1/*T* and the insert represents *ln*(τ) vs. 1/(*T*-T_o). T_o is adjustable parameter. The symbol represents the experimental data points and the solid line is the least square linear fit to VTF equation.

mesostructure. Because the mobile alkali ions in the mixed bioactive glass create a polarization system by reorienting locally, and are also responsible for conduction by separating itself from the immediate neighbourhood [29].

In order to further elucidate the dielectric relaxation in bioglass composite, it is important to estimate the activation energy associated with the relaxation process which could be obtained from the temperature dependence of relaxation times. Figure 6 shows the logarithms of relaxation time dependence of the inverse of temperature. It is clear from this figure that, below T_g the temperature dependence of relaxation times typically follows the Vogel-Tammam-Fulcher (VTF), this latter has also been experimentally observed in a variety of super cooled organic liquids, polymers and bioglasses which is characteristic of cooperative relaxations [29-32].

$$\ln\left(\frac{\tau}{\tau_0}\right) = \frac{w}{k_B(T - T_{VF})} \quad (5)$$

where τ_o is the relaxation time in the high temperature limit, k_B is the Boltzmann constant and T_{VF} is an ordering temperature below T_g. W is directly related to activation energy. If we regard that the VTF law describes a thermally activated process, the W is approaching infinity at T_{VF}.

In Equation 5 the non-Arrhenius behaviour is taken into account by introducing the Vogel-Fulcher temperature T as an additional parameter leading to a divergence at T = T_{VF}. This divergence may be taken as indication of a phase-transition-like "ideal" flass transition that would occur at a temperature T_{VF} below the glass temperature T_g, which, however, is avoided for dynamical reasons. It provides some support to theories that assume such a transition underlying the evolution of the glass state [18,24].

The best fit of our data using maximum likelihood yields $\tau_o \approx 8.03\ 10^{-9}$ s, $T_{VF} \approx 220$K which an ordering temperature lower than the T_g whose significances has remained unclear (there is no microscopic presentation to calculate T_{VF}), and free energy of thermal activation energy W=58.08 *meV* with a correlation coefficient of R=0.998 which we interpret as the average potential barrier between different sites inside the network heterostructure. The obtained value of W is very smaller than the data of Dutta et al. [29] those investigated the dielectric relaxation of the Na_2O-CaO-Si_2O system with various concentrations of alkali ions, this difference may be related to the effect of phosphate (P_2O_5) that is added in this study, on the rigidity of network mesostructure which caused the decreases in activation energy.

Conclusion

The effective complex permittivity of bioactive glass composite was studied over a frequency range from 100 Hz to 1 MHz and in a temperature range from 100 to 370 K by impedance spectroscopy. This study exhibits typical dielectric relaxation process which was modelled using the Havriliak–Negami phenomenological. The analysis of the temperature dependence of their relaxation time using the Vogel-Tamman- Fulcher (VTF) model shows a weak interaction in the bioactive network.

References

1. Larry LH (2013) Chronology of bioactive glass development and clinical applications. New Journal of Glass and Ceramics 3: 67-73.
2. Thamboon P, Krol DM (2003) Second-order optical nonlinearities in thermally poled phosphate glass. J Appl Phys 93: 32-37.
3. Mingxin Q, Vilaseca R, Botey M, Sellarès J, Pi F et al. (2000) Double fitting of maker fringes to characterize near-surface and bulk second-order nonlinearities in poled silica. Appl Phys Lett 76: 3346-3348.
4. Obata A, Nakamura S, Moriyoshi Y, Yamashita K (2003) Electrical polarization of bioactive glass and assessment of their in vitro apatite deposition. J Biomed Mater Res A 67: 413-420.
5. Bini M, Grandi S, Capsoni D, Mustarelli P, Saino E, et al. (2009) SiO_2−P_2O_5−CaO glasses and glass-ceramics with and without ZnO: Relationships among composition, microstructure, and bioactivity. J Phys Chem 113: 8821-8828.
6. Hench LL (1991) Bioceramics: From concept to clinic. J Amer Cer Soc 74: 1487-1510.
7. Neo M, Nakamura T, Ohtsuki C, Kokubo T, Yamamuro T (1993) Apatite formation on three kinds of bioactive material at an early stage in vivo: a comparative study by transmission electron microscopy. J Biomed Mater Res 27: 999-1006.
8. Knowles JC (2003) Phosphate based glasses for biomedical applications. J Mater Chem 13: 2395-2401.
9. Ahmed I, Collins CA, Lewis M, Olsen I, Knowles JC (2004) Processing, characterization and biocompatibility of iron-phosphate glass fibres for tissue engineering. Biomater 25: 3223-3332.
10. Bitar M, Knowles JC, Lewis MP, Salih V (2005) Soluble phosphate glass fibres for repair of bone-ligament interface. J Mater Sci Mater Med 16: 1131-1136.
11. Carta D, Pickup DM, Knowles JC, Ahmed I, Smith ME, et al. (2007) A structural study of sol–gel and melt-quenched phosphate-based glasses. J Non-Cryst Solids 353: 1759-1765.
12. Kulkarni AR, Lunkenheimer P, Loidl A (1998) Scaling behaviour in the frequency dependent conductivity of mixed alkali glasses. Solid State Ionics 112: 69-74.

13. Mai C, Etienne S, Perez J (1985) Modulus and internal friction in phosphate-silicate bioactive glass. J Non- Cryst Solids 74: 119-127.

14. Mariappan CR, Roling B (2010) Mechanism and kinetics of Na+ ion depletion under the anode during electro-thermal poling of a bioactive glass. J Non- Cryst Solids 356: 720-724.

15. Maheswaran A, Hiran Kumar G, Karthick Prabhu S, Daries Bella RS (2012) Effect of annealing temperatures on an ion transport properties of the bioglass. J Alloy Compd 532: 86-91.

16. Maheswaran A, Hiran Kumar G, Nithya H, Karthick Prabhu S, Junichi K (2014) Structure, dielectric and bioactivity of P_2O_5–CaO–Na_2O–B_2O_3 bioactive glass. Applied Physics A 117: 1323-1327.

17. Hasnaoui MEl, Triki A, Graça MPF, Achour ME, Costa LC, et al. (2012) Electrical conductivity studies on carbon black loaded ethylene butylacrylate polymer composites. J Non- Cryst Solids 358: 2810-2815.

18. Ediger MD, Angell CA, Nagel SR (1996) Supercooled liquids and glasses. J Phys Chem 100: 13200-13212.

19. Ngai KL (2000) Dynamic and thermodynamic properties of glass-forming substances. J Non- Cryst Solids 275: 7-51.

20. Dyre JC (2006) The glass transition and elastic models of glass-forming liquids. Rev Mod Phys 78: 95.

21. Schneider U, Lunkenheimer P, Pimenov A, Brand R, Loidl A (2001) Wide range dielectric spectroscopy on glass-forming materials: An experimental overview. Ferroelectrics 249: 89.

22. Roland CM, Hensel-Bielowka S, Paluch M, Casalini R (2005) Supercooled dynamics of glass-forming liquids and polymers under hydrostatic pressure. Rep Prog Phys 68: 1405-1478.

23. Wehn R, Lunkenheimer P, Loidl A (2007) Broadband dielectric spectroscopy and aging of glass formers. J Non-Cryst Solids 353: 3862-3870.

24. Angell A (1984) Relaxations in complex systems. National Technical Information Service, Springfield.

25. Fulcher GS (1925) Introduction to glass science and technology. J Am Ceram Soc 8: 339.

26. Sural M, Ghosh A (2000) Electric conductivity and relaxation in ZnF2–AlF3–PbF2–LiF glasses. Solid State Ionics 130: 259-266.

27. Arora A, Shaaban ER, Singh K, Pandey OP (2008) Non-isothermal crystallization kinetics of ZnO–BaO–B_2O_3–SiO_2 glass. J Non- Cryst Solids 354: 3944-3951.

28. Ryabov Ya E, Yuri F (2002) Novel approach to the analysis of the non-Debye dielectric spectrum broadening. Physica A 314: 370-378.

29. Dutta A, Sinha TP, Jena P, Adak S (2008) AC conductivity and dielectric relaxation in ionically conducting soda–lime–silicate glasses J Non- Cryst Solids 354: 3952-3957.

30. Kaur N, Singh M, Singh A, Awasthi AM, Snigh L (2012) Dielectric relaxation spectroscopy of phlogopite mica. Physica B 407: 4489-4494.

31. Fritzsche J, Das A, Jurk R, Stockelhuber KW, Heinrich G, et al. (2008) Relaxation dynamics of carboxylated nitrile rubber filled with organomodified nanoclay. expr Polym Lett 2: 373-381.

32. Jonscher AK (1999) Dielectric relaxation in solids. J Phys D Appl Phys.